DINAME 2017 - Proceedings of the XVII International Symposium on Dynamic Problems of Mechanics
A. T. Fleury, D. A. Rade, P. R. G. Kurka (Editors), ABCM, São Sebastião, SP, Brazil, March 5-10, 2017

DINAME 2017 - Evaluation of the dynamic response of buildings with TMDs under earthquakes

Rúbia M. Bosse[1], **André Teófilo Beck**[1]

[1] University of São Paulo – Structural Engineering Department. Av. Trabalhador Sancarlense, 400, 13566-590, rubiabosse@usp.br, atbeck@sc.usp.br

Abstract: The structural system of buildings with tuned mass dampers (TMDs) is usually approximated as a set of concentrated masses, representing the floors, connected by linear springs, representing the columns. This paper shows that such spring-mass approximations can be very inaccurate for the prediction of the structural response and for the determination of optimal TMD parameters. In this way, a positional finite element model is developed, and employed to evaluate linear and geometrically nonlinear dynamical responses of building structures with TMDs under the El Centro earthquake. It was noted that TMDs tuned to higher frequencies work better at minimizing displacements and oscillation frequency, in contrast to what is popularly believed, that devices tuned to the building's fundamental frequencies present ideal performance. The linear regimen showed to be sufficient to estimates the displacements of the building and the imposition of earthquake loads as equivalent lateral forces was not representative and does not describe accurately the behavior of the structure. The incorporation of TMDs showed to be very effective in reducing vibrations when the structure is subjected to El Centro earthquake loads. However, benefits are only achieved when the TMDs are properly tuned, and when structural responses are correctly evaluated. Simple lumped spring-mass models are very limited in predicting structural responses under earthquake excitations.

Keywords: TMD, Dynamic response, Geometrical nonlinear analysis, tuning frequency, earthquake.

INTRODUCTION

Techniques and devices to suppress structural vibrations have been developed to enable safe solutions to tall building design. In this subject, the passive vibration control with Tuned Mass Dampers (TMDs) has the advantage of being simple and efficient in reducing the dynamic motion of structures, without demanding external power sources (Housner et al., 1997; Spencer and Nagarajaiah, 2003). The classic TMD is a vibration absorber composed by an auxiliary mass, connected to a linear spring, placed in parallel with a viscous damping device, commonly attached to the top of the building. Conventionally, tuning the frequency of the device to the first natural frequency of the structure is believed to lead to optimal performance.

TMDs were first studied in 1909 by Frahm (1909). Few decades later, the devices began to be employed in buildings. Den Hartog (1928) performed first studies on optimal TMD design, developing analytical expressions for one degree of freedom systems (1DOF). Later, Warburton and Ayorinde (1980) further advanced the subject by considering damping in the main system. Warburton (1982) also considered random loads acting on the structure, and proposed a formulation to treat MDOF systems as an equivalent 1DOF system. Surely, when dealing with multiple degrees-of-freedom (MDOF) structures, and with uncertainties in loads, the absorber showed to be less effective in mitigating vibrations and it was found that the performance of absorbers is sensible to tuning parameters and damping coefficient, thus many strategies have been developed to enhance the performance of TMDs (Rana and Soong 1998; Kaynia et al., 1981; Hoang and Warnitchai 2005; Marian and Giaralis 2015; Rüdinger 2006; Tubaldi and Kougiomtzoglou 2014).

In general, TMDs have been successfully employed to reduce vibrations induced by wind forces; this is due to the fact that winds usually present a limited range of excitation frequencies. In this aspect, the TMDs are designed to control the first mode of the structure and tuned to the fundamental natural frequency of the building, which is more susceptible to be excited by winds. However, earthquakes can include a wide spectrum of excitation frequencies; hence there is no general agreement about the performance of TMDs to mitigate seismic-induced oscillations. It was found that the reduction of displacements in the main structure is dependent on the ground motion frequency (Hoang et al., 2008; Housner et al. 1997; Parulekar and Reddy 2009; Rana and Soong 1998; Soto-brito and Ruiz 1999).

Most researches in vibration control model building structures as discrete mass-spring-damper systems (Pourzeynali et al., 2007; Hoang et al., 2008; Moutinho, 2012; Beck et al., 2014; Lazar et al., 2014; Miguel et al, 2016) and evaluate their dynamical responses in linear regimen, usually by modal superposition. In such approaches, the TMD is represented as an additional DOF attached to the main structure. Such lumped spring-mass models can be considered limited, because they assume structural members as non-deformable bodies, hence they cannot properly account for large deflections. Tall buildings are very sensitive to structural vibrations, and often present large displacements,

especially under earthquake-induced base motion.

This paper presents a methodology to obtain accurate and realistic dynamical responses of building structures equipped with TMDs, and subject to earthquake ground motions. A positional finite element (FE) formulation is employed to evaluate linear and geometrically nonlinear dynamical responses. Optimal TMD design is considered, for building structures subject to the 1940 El Centro earthquake loading.

Positional finite element and mass-spring model

Geometrical nonlinear analysis is used to handle large deflections: the structure's equilibrium position in sought on its displaced state. In the so-called positional FE approach, a non-dimensional space is created and the relative curvature of beam elements is calculated for the initial and for the deformed configurations (Coda and Greco 2004). The equilibrium position is the main unknown variable, and it is obtained from the principle of stationary total potential energy. A total Lagrangian formulation is employed, using an unique reference configuration, the initial position; in this context, the mass matrix is constant and a frame element with four nodes and cubic approximation is employed. The system of nonlinear equations is solved combining the Newmark time integration with the Newton-Raphson procedure, following Coda and Paccola (2014).

The linear analysis differs from the nonlinear because equilibrium is calculated in the initial position, presenting a constant stiffness matrix. In this way, the linear equilibrium equations are solved applying the Newmark time integration considering constant average acceleration, according to Paultre (2010) and Warburton (1976).

In the classical mass-spring model, the mass of each storey represents one degree of freedom, and spring stiffness is determined by the sum of the stiffness of all floor columns (Warburton, 1976). All connections are assumed rigid, the system is linear, the slabs are non-deformable and the lateral displacements are due to column flexibility. The assembling of mass, stiffness and damping matrices can be consulted in Paultre (2010).

Frame positional FE model

Initially, it is necessary to map the initial and current configurations of the beam finite element from the reference line. The tangent $\left(\boldsymbol{t}_{ik}\right)$ and normal vectors $\left(\boldsymbol{v}_{1k},\boldsymbol{v}_{2k}\right)$ of the nodes are presented in Eq. (1), according to Fig. 1:

$$\boldsymbol{t}_{ik}=\left.\frac{\boldsymbol{d}\varphi\left(\xi\right)}{\boldsymbol{d}\xi}\right|_{\xi_k}\boldsymbol{X}_{il}^{\boldsymbol{m}},\quad \boldsymbol{v}_{1k}=\frac{-\boldsymbol{t}_{2k}}{\sqrt{\boldsymbol{t}_{ik}\boldsymbol{t}_{ik}}},\quad \boldsymbol{v}_{2k}=\frac{-\boldsymbol{t}_{1k}}{\sqrt{\boldsymbol{t}_{ik}\boldsymbol{t}_{ik}}}, \tag{1}$$

where $\boldsymbol{i}$ is the coordinate direction, $\boldsymbol{m}$ represents the reference line, $\boldsymbol{l}$ the element node (shape function), ξ_k are the non-dimensional coordinates of the nodes, φ are the shape functions. Figure 1 shows the initial angle between the normal vector and the horizontal direction $\boldsymbol{x}_1$:

$$\theta_k^0=\operatorname{arctg}\left(\frac{\boldsymbol{v}_{2k}}{\boldsymbol{v}_{1k}}\right), \tag{2}$$

Using the shape functions (Lagrange polynomials) to approximate $\theta^0\left(\xi_1\right)$, one obtains:

$$\theta^0\left(\xi\right)=\varphi_\ell\left(\xi\right)\theta_\ell^0. \tag{3}$$

It is possible to define the position of any point inside the element, by the vector $\boldsymbol{g}_i^0\left(\xi,\eta\right)$, according to Figure :

$$\boldsymbol{x}_i\left(\xi,\eta\right)=\boldsymbol{x}_i^{\boldsymbol{m}}\left(\xi\right)+\boldsymbol{g}_i^0\left(\xi,\eta\right),\quad \boldsymbol{g}_1^0\left(\xi,\eta\right)=\frac{\boldsymbol{h}_0}{2}\eta\cos\left[\varphi_\ell\left(\xi\right)\theta_\ell^0\right],\quad \boldsymbol{g}_2^0\left(\xi,\eta\right)=\frac{\boldsymbol{h}_0}{2}\eta\boldsymbol{sen}\left[\varphi_\ell\left(\xi\right)\theta_\ell^0\right], \tag{4}$$

where, η are the non-dimensional variables along the height $\boldsymbol{h}_0$.

In this way, the complete mapping is obtained for both directions as:

$$\boldsymbol{f}_1^0\left(\xi,\eta\right)=\varphi_\ell\left(\xi\right)\boldsymbol{X}_1^\ell+\frac{\boldsymbol{h}_0}{2}\eta\cos\left[\varphi_\ell\left(\xi\right)\theta_\ell^0\right],\ \boldsymbol{f}_2^0\left(\xi,\eta\right)=\varphi_\ell\left(\xi\right)\boldsymbol{X}_2^\ell+\frac{\boldsymbol{h}_0}{2}\eta\boldsymbol{sen}\left[\varphi_\ell\left(\xi\right)\theta_\ell^0\right]. \tag{5}$$

The current configuration is the unknown parameter of the problem: it is obtained by an iterative process. However, in the first step it is assumed that the current configuration is equal to the initial one. The current configuration is defined by:

$$\boldsymbol{f}_1^1\left(\xi,\eta\right)=\varphi_\ell\left(\xi\right)\boldsymbol{Y}_1^\ell+\frac{\boldsymbol{h}_0}{2}\eta\cos\left[\varphi_\ell\left(\xi\right)\theta_\ell\right],\ \boldsymbol{f}_2^2\left(\xi,\eta\right)=\varphi_\ell\left(\xi\right)\boldsymbol{Y}_2^\ell+\frac{\boldsymbol{h}_0}{2}\eta\boldsymbol{sen}\left[\varphi_\ell\left(\xi\right)\theta_\ell\right], \tag{6}$$

where, $\boldsymbol{Y}_i^\ell$ are the current coordinates, φ_ℓ current angles of the cross section.

With the mappings from the non-dimensional space to initial and current configurations defined, the deformation of the element can be described by the change of configuration function as (Fig. 3):

$$\vec{\boldsymbol{f}}=\vec{\boldsymbol{f}}_1\circ\left(\vec{\boldsymbol{f}}_0\right)^{-1} \tag{7}$$

The gradient of this function is obtained from the mapping gradients:

$$\mathbf{A} = \mathbf{A}^1.\left(\mathbf{A}^0\right)^{-1},\ \mathbf{A}^0 = \begin{bmatrix} \frac{\partial \boldsymbol{f}_1^0}{\partial \xi} & \frac{\partial \boldsymbol{f}_1^0}{\partial \eta} \\ \frac{\partial \boldsymbol{f}_2^0}{\partial \xi} & \frac{\partial \boldsymbol{f}_2^0}{\partial \eta} \end{bmatrix},\ \mathbf{A}^1 = \begin{bmatrix} \frac{\partial \boldsymbol{f}_1^1}{\partial \xi} & \frac{\partial \boldsymbol{f}_1^1}{\partial \eta} \\ \frac{\partial \boldsymbol{f}_2^1}{\partial \xi} & \frac{\partial \boldsymbol{f}_2^1}{\partial \eta} \end{bmatrix}. \tag{8}$$

To calculate the geometrically exact position, the objective Green-Lagrange strain measure is used:

$$\mathbf{E} = \frac{1}{2}\left(\mathbf{C} - \mathbf{I}\right) = \frac{1}{2}\left(\mathbf{A}^{\prime} \cdot \mathbf{A} - \mathbf{I}\right), \tag{9}$$

where $\mathbf{I}$ is the (2x2) identity tensor and $\mathbf{C}$ is the right Cauchy stretch.

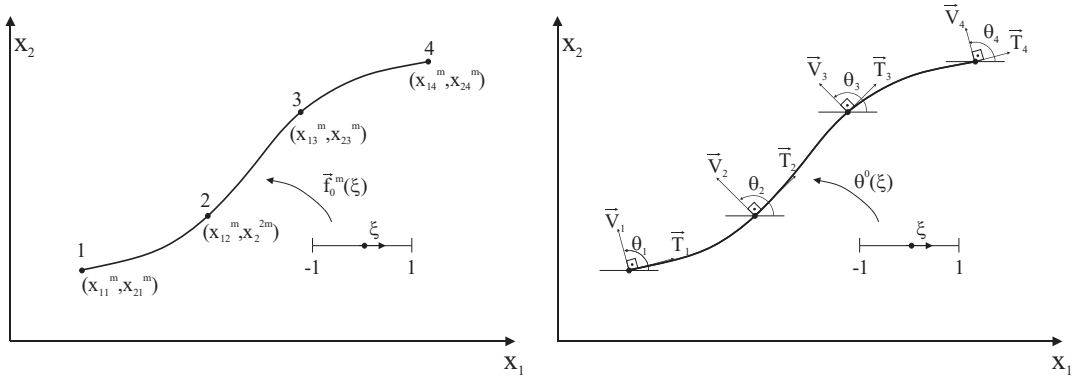

Figure 1 - Nodal vectors and reference line of the beam finite element, cubic approximation (Coda and Paccola 2014).

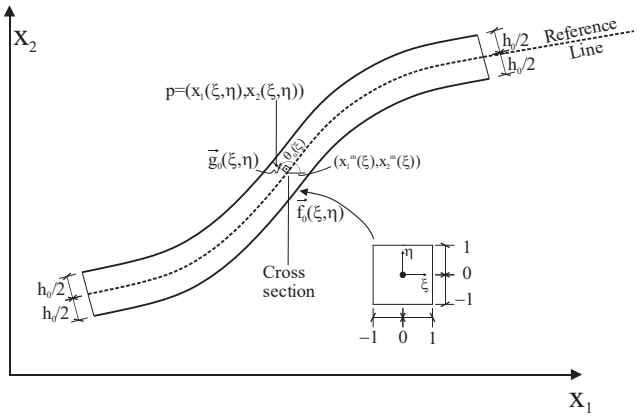

Figure 2 – Cross section point (Silva, 2010)**.**

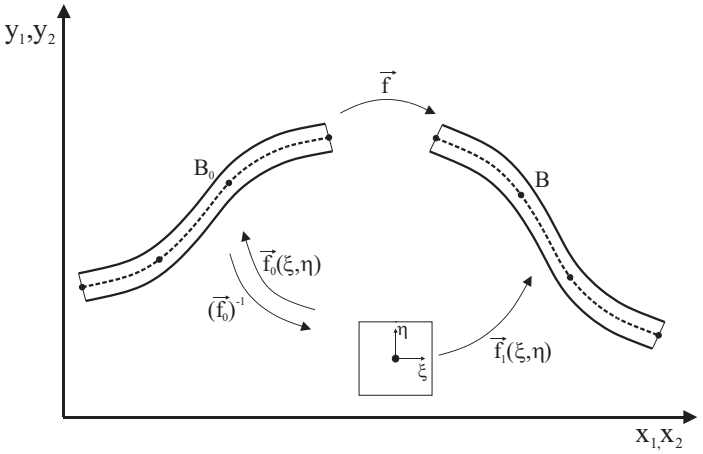

Figure 3 – Change of configuration (Coda and Paccola 2014).

Geometrically nonlinear elasto-dynamics

The Saint-Venant-Kirchhoff specific strain energy is employed to relate the Green strain $(\mathbf{E})$ and the second Piola-Kirchhoff stress $(\mathbf{S})$:

$$\boldsymbol{u_e} = \frac{\mathrm{E}}{2}\left\{\left(\boldsymbol{E}_{11}^2 + \boldsymbol{E}_{22}^2\right) + \boldsymbol{G}\left(\boldsymbol{E}_{12}^2 + \boldsymbol{E}_{21}^2\right)\right\}, \tag{10}$$

where E is the longitudinal elasticity modulus for small deformations, $\boldsymbol{E_{ij}}$ is the Green strain tensor, and $\boldsymbol{G} = \boldsymbol{E}/[2(1+\upsilon)]$. By considering the Poisson ratio υ to be zero, volumetric locking is avoided.

The strain energy stored in the elements can be written as:

$$\boldsymbol{U_e}\left(\vec{\boldsymbol{Y}}\right) = \int_{V_0} \boldsymbol{u_e}\left(\vec{\boldsymbol{Y}}\right) \boldsymbol{dV_0}, \tag{11}$$

where $\boldsymbol{V_0}$ is the initial volume of the structure.

The total energy of the system is obtained by adding the parcels due to the potential energy of external loads, kinetic energy, potential of external distributed forces, viscous damping and strain energy of the frame elements:

$$\prod(\vec{\boldsymbol{Y}}) = \int_{V_0} \boldsymbol{u_e}(\vec{\boldsymbol{Y}})\, \boldsymbol{dV_0} - \vec{\boldsymbol{F}} \cdot \vec{\boldsymbol{Y}} - \int_{S_0} \boldsymbol{q} \cdot \vec{\boldsymbol{y}}^{\boldsymbol{m}}\, \boldsymbol{dS_0} + \frac{1}{2}\int_{V_0} \rho_0 \dot{\vec{\boldsymbol{y}}} \cdot \dot{\vec{\boldsymbol{y}}}\, \boldsymbol{dV_0} + \boldsymbol{Q}, \tag{12}$$

where $\vec{\boldsymbol{F}}$ is the external nodal force vector, $\boldsymbol{q}$ is the general distributed force vector, $\vec{\boldsymbol{y}}^{\boldsymbol{m}}$ is the current position, $\dot{\vec{\boldsymbol{y}}}$ is the velocity, $\boldsymbol{dS_0}$ the infinitesimal element's length, $\boldsymbol{Q}$ is the viscous damping.

The principle of stationary potential energy is applied to the total energy of the system, to impose the equilibrium of the structure:

$$\partial \prod\left(\vec{\boldsymbol{Y}}\right) = \vec{\boldsymbol{F}}^{\mathrm{int}} \cdot \partial \vec{\boldsymbol{Y}} - \vec{\boldsymbol{F}} \cdot \partial \vec{\boldsymbol{Y}} - \mathbf{L} \cdot \vec{\boldsymbol{Q}} \cdot \partial \vec{\boldsymbol{Y}} + \mathbf{M} \cdot \ddot{\vec{\boldsymbol{Y}}} \cdot \partial \vec{\boldsymbol{Y}} + \mathbf{D} \cdot \dot{\vec{\boldsymbol{Y}}} \cdot \partial \vec{\boldsymbol{Y}} = \vec{0}, \tag{13}$$

where $\vec{\boldsymbol{F}}^{\mathrm{int}}$ refers to the internal force vector, $\mathbf{L}$ is the matrix used to transform distributed loads into equivalent nodal ones, $\mathbf{M}$ is the constant mass matrix, $\mathbf{D}$ is the mass-proportional damping matrix. Eq. (13) represents the geometrical nonlinear dynamic equilibrium equation because of the arbitrariness of vector $\partial \vec{\boldsymbol{Y}}$.

Assembled the mass and damping matrixes of the structure, and established the initial and current configuration of the elements, a temporal integration combined with the resolution of the non-linear equations is made. The resolution of the system implies the iterative calculus of the internal loads vector, the hessian matrix and update of the positions in each time step.

Vector $\vec{\boldsymbol{g}}$ is the vector of unbalanced mechanical forces, it is null if $\vec{\boldsymbol{Y}}$ is the correct trial position, used to calculate internal forces. The dynamic equilibrium is obtained by solving, for any time:

$$\vec{\boldsymbol{g}} = \vec{\boldsymbol{F}}^{\mathrm{int}} - \vec{\boldsymbol{F}} + \mathbf{M} \cdot \ddot{\vec{\boldsymbol{Y}}} + \mathbf{D} \cdot \dot{\vec{\boldsymbol{Y}}} = \vec{0}. \tag{14}$$

The resulting nonlinear system is time-integrated by the Newmark method and linearized by the Newton-Raphson algorithm; the complete technique can be consulted in Coda and Paccola, (2014). The iterative process ends when a stopping tolerance $(\boldsymbol{Tol})$ is satisfied, representing the correct equilibrium position.

$$\frac{\left\|\vec{\boldsymbol{g}}\left(\vec{\boldsymbol{Y}}_{\boldsymbol{s}+1}\right)\right\|}{\left\|\vec{\boldsymbol{F}}\right\|} \le \boldsymbol{Tol}. \quad \textbf{\textit{and}} \quad \frac{\left\|\Delta\vec{\boldsymbol{Y}}_{\boldsymbol{s}+1}\right\|}{\left\|\vec{\boldsymbol{X}}\right\|} \le \boldsymbol{Tol}, \tag{15}$$

where $\Delta\vec{\boldsymbol{Y}}_{\boldsymbol{s}+1}$ is the current incremental displacement and $\vec{\boldsymbol{X}}$ is the initial position.

RESULTS AND DISCUSSION

Building subject of the study

In the results session to follow, a 20-storey building was modelled, to evaluate its dynamical response under the El Centro Earthquake. Modal analysis were performed to obtain the natural frequencies and vibration modes of the structure, which was discretized using two models: mass-spring and plane frame FE models. The TMD was attached to the last floor of the building and the dynamic responses were compared for three regimens of analyses: linear with equivalent forces applied to nodal degrees-of-freedom, linear with base motion and geometrically nonlinear with ground motion.

The building under study has 20 stores, total 72 meters of height, and is composed by columns and beams. The structural elements have the dimensions indicated in Fig. 4 (a). One sample of the El Centro accelerogram is shown in Fig. 4 (b).

For the FE model, the structure was discretized into 200 4-node frame elements; these elements can describe translations in horizontal and vertical direction, and the angle between the tangent and normal vectors of the nodes. For the mass-spring model, the building is represented by 20 non-deformable masses, and only horizontal displacements are evaluated. Equivalent properties of the mass-spring building model are shown in Table 1. Details about the mass-spring model, and about model equivalence, are described in references Pourzeynali et al. (2007) and Lazar et al.(2014).

For the FE model, a distributed vertical load of 4KN/m was considered representing the live loads and a solid concrete slab of 15cm contributes to the mass of the building. The connection between columns and beams is rigid, and the natural damping of the building was disregarded. The adopted material is reinforced concrete, with longitudinal elastic modulus of 40GPa, transversal elastic modulus of 20GPa, density of 2500Kg/m³. The time of simulation was 32 seconds, the time step adopted was $\Delta t = 0.02s$.

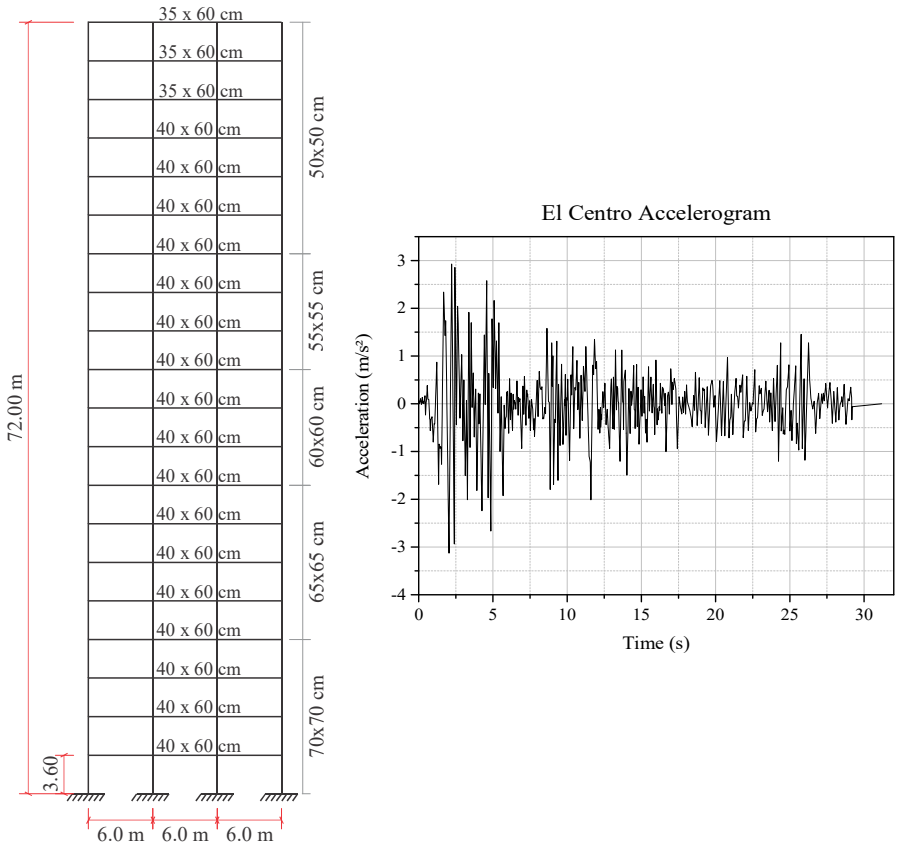

Figure 4 (a) Dimensions of the building and its elements;(b) El Centro Accelerogram.

Table 1 - Properties of the mass-spring building model.

Storey	M_{Beams} (Kg) $b.h.l.\rho$ *	$M_{Columns}$ (Kg) $b.h.l.\rho.n$ *	$K_{Columns}$ (MN/m) $12EI / L^3$ *	$M_{Equiv.}$ (Kg) $M_{Beams} + M_{Columns}$	$K_{Equiv.}$ (MN/m) $\sum K_{Columns}$
18-20	9450	9000	0.0536	18450	0.2143
15-17	10800	9000	0.0536	19800	0.2143
12-14	10800	10890	0.0785	21690	0.3138
9-11	10800	12960	0.1111	23760	0.4444
5-8	10800	15210	0.1530	26010	0.6122
1-4	10800	17640	0.2058	28440	0.8234

* b and h are the dimensions of the elements presented in Fig. 4(a); L is the total length of beams and columns; ρ is the material density; n is the number columns of each floor; E is the elastic modulus of the material; I is the moment of inertia of the columns' cross section.

Natural frequencies

To determine the natural frequencies of the building, modal analysis was employed, were calculated the natural frequencies for both models (spring-mass and finite element discretization) the results are shown in Table 2, the modes of vibration were determined by the eigenvectors of the system and are presented in Fig. 5.

It can be observed that the vibration modes for the models (mass-spring and FE) tend to be similar, while the natural frequencies corresponding to these modes are different for the two models of discretization. Since the FE model involves a better discretization and a higher number of DOF, it is considered more accurate. Hence, it becomes clear that the mass-spring model has significant limitations with regards to the determination of the buildings natural frequencies.

Table 2 – First 10 natural frequencies of the building.

Mass-Spring - Freq. (Hz)	FE model - Freq. (Hz)
1.95	0.55
4.72	1.57
7.87	2.73
10.95	3.91
13.71	5.13
16.64	6.41
19.50	7.15
22.48	7.86
24.73	8.96
26.93	9.29

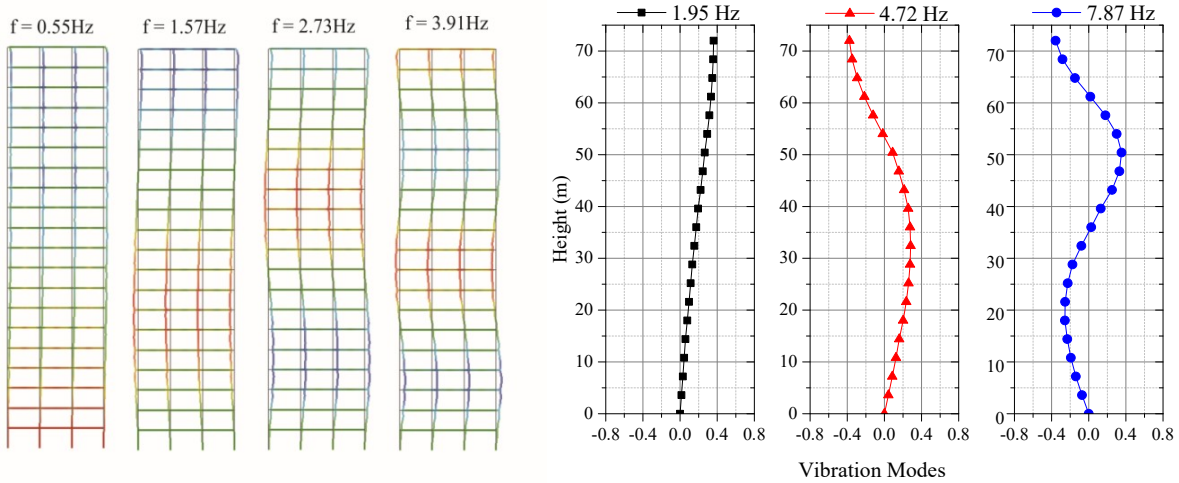

Figure 5 - Vibration modes for the FE model and mass-spring model.

TMD tuning frequencies

It is well established in the literature that TMDs perform well when their frequency is tuned to the first natural frequency of the building. When the first mode of vibration is excited by wind loads, for instance, the vibration energy is transferred from the building to the TMD.

Wind loads have a narrow spectrum of frequencies, which can be close to the first natural frequencies of the building. Earthquake loading, however, poses a different challenge, as excitation frequencies are broad-banded; hence, in principle, many vibration modes of a structure can be excited. For this reason, there is no general agreement about optimal TMD design, or about their efficiency, in reducing vibrations induced by seismic loading. If the TMD is tuned to the structure's fundamental frequency, the absorber will substantially reduce just the response of the first mode, without affecting the vibration in higher modes (Parulekar and Reddy, 2009).

In this paper, a study about the tuning of TMD frequency is developed. The TMD is employed in the 20 story building described above, and subject to El Centro earthquake record. Three finite element models were studied, to evaluate appropriateness of modelling assumptions:

a) Linear analysis with equivalent horizontal nodal loads applied along the buildings height;
b) Geometrical nonlinear analysis (GNL) and linear analysis with base-imposed earthquake displacements.

The simplified mass-spring model is also considered, mainly to compare its response with the distributed load linear FE model.

The TMD was modelled as an additional frame rigid element placed at the last storey; the element is 60cm long and is connected to the building by two linear frame elements, whose axial stiffness is calibrated to yield the required natural frequency for the TMD. TMDs tuned to the first 10 natural frequencies of the building were tested. For the mass-spring model, the TMD was considered as an additional mass connected to the last DOF of the structure.

For the present tuning frequency study, the mass ratio was fixed at $\bar{m} = 0.01$; and the design of the TMD was determined according to the simplified Eqs. (16), (17), (18) as shown in (Rana and Soong, 1998), and with the modal generalized mass and stiffness properties corresponding to each mode of vibration of the structure:

$$f_{opt} = \frac{1}{1+\bar{m}}\left(\sqrt{\frac{2-\bar{m}}{2}}\right),\ \xi_{opt} = \sqrt{\frac{3\bar{m}}{8(1+\bar{m})}}\left(\sqrt{\frac{2}{2-\bar{m}}}\right),\ \omega_{TMD} = f_{opt}\omega_{Struc.}\ , \tag{16}$$

$$m_{TMD} = \bar{m}m_{Struc.},\ K_{opt} = \omega_{TMD}^2 m_{TMD},\ C_{opt} = 2\omega_{TMD}\xi_{opt}m_{TMD.} \tag{17}$$

$$M_{gen.} = \varphi_i^T \mathbf{M}\varphi_i,\ K_{gen.} = \varphi_i^T \mathbf{K}\varphi_i, \tag{18}$$

where, f_{opt} is the optimal frequency, ξ_{opt} is the TMD optimal damping ratio, ω_{TMD} is the TMD natural frequency, ω_{Struc} is the natural frequency of the structure, m_{TMD} is the TMD mass, $m_{Struc.}$ is the total mass of the main structure, K_{opt} is the optimal TMD stiffness, C_{opt} is the optimal TMD damping, M is the mass matrix of the structure, K the stiffness matrix of the structure, φ_i is the mode of vibration vector corresponding to the natural frequency of the structure in analysis. Table 3 presents the TMDs parameters designed to reduce the response of the firsts 10 modes of vibration of the building.

In Figs 6-9, the horizontal displacements at the top of the building can be observed, for the different tuning frequencies of the TMDs.

Table 3 – TMD designs.

Mode of vibration	$\omega_{Struc} = \omega_{FE\ model}$ (rad/s)	$M_{gener.}$ 10^3	$K_{gener.}$ 10^8	ω_{Opt} (rad/s)	$K_{opt.}$ 10^7 (N/m)	C_{Opt} 10^5
1	3.46	2.10	10.1	3.07	0.0095	0.21
2	9.86	2.11	9.38	8.74	0.0771	0.59
3	17.18	2.12	9.51	15.22	2.34	1.02
4	24.56	2.12	9.63	21.76	4.78	1.46
5	32.21	2.13	9.64	28.54	8.22	1.91
6	40.29	2.13	9.58	35.70	12.86	2.39
7	44.91	2.14	11.14	39.80	15.98	2.67
8	49.40	2.12	9.78	43.77	19.33	2.93
9	56.28	2.10	10.41	49.86	25.08	3.34
10	58.40	2.12	9.78	51.74	27.01	3.47

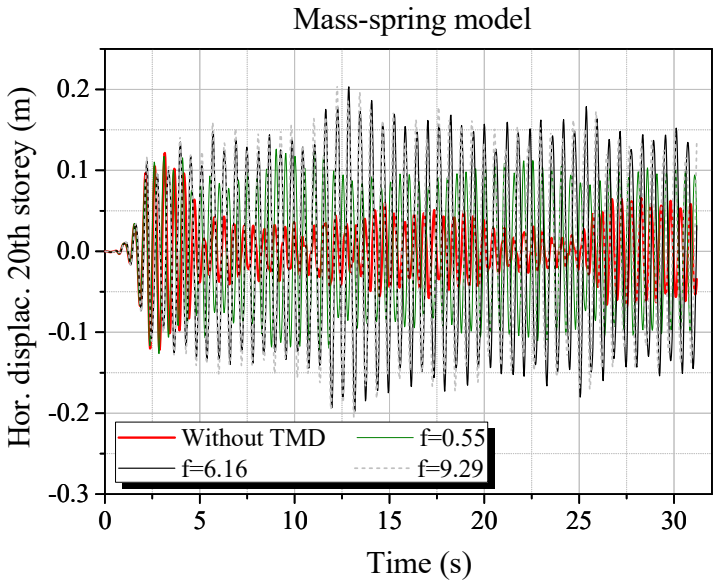

Figure 6 – Response of mass-spring model at 20th DOF, without and with TMDs tuned to different frequencies "f".

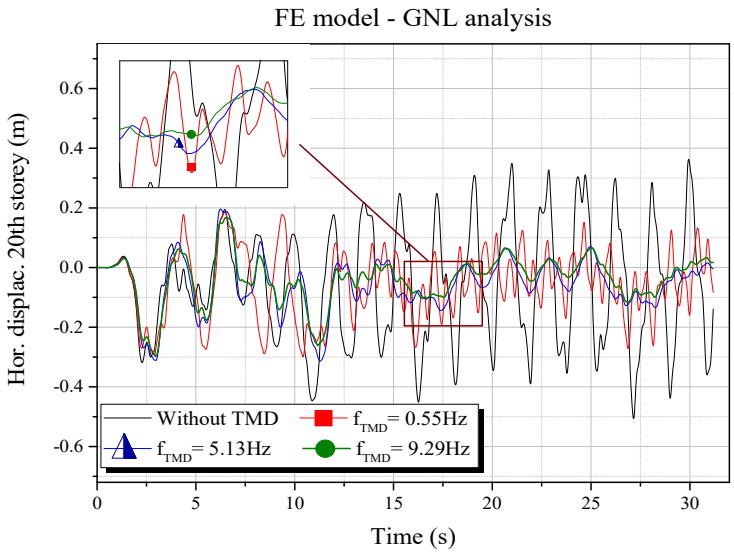

Figure 7 – Response of GNL model, at 20th storey, without and with TMDs tuned to different frequencies "f".

Figure 6 shows that the mass-spring model is inaccurate to represent structural responses for the TMD-equipped building. Displacements obtained with the mass-spring model are much smaller than displacements obtained with the FE model.

In Fig. 7, responses of the non-linear FE model are shown; however, for this example, linear responses are identical. Figure 7 shows that TMDs are efficient at suppressing structural vibrations. It can also be observed that TMDs tuned to higher frequencies (i.e. 9.29Hz) have better performance.

Figure 8 compares the responses of the four models studied in this section, for the structure without TMD, and with TMDs tuned to different frequencies. It can be observed that, for the structure without TMD, responses of the three FE analysis models (linear with equivalent loads, linear with base displacements and geometrically nonlinear with base displacements) are equivalent, presenting the same frequency of oscillation and closely matching displacements. This shows that displacements for the structure without TMD are not too large, and can be accurately described by a linear FE analysis, and event for a simplified load model

In Fig. 8, it also becomes clear that the equivalent load model significantly overrate structural displacements; turning this model inadequate to represent structural responses under seismic loadings. It can be also observed that for higher tuning frequencies, the TMD-building system becomes stiffer, displacements and oscillation frequency are significantly reduced, and for all cases the linear and non-linear models tend to agree.

Figure 9**Figure** presents a comparison between the El Centro displacements imposed to the structure's base and the last floor's displacements of the TMD equipped building. Two structural responses are shown in the Figure; with a TMD tuned to $f = 0.55Hz$ and $f = 9.29Hz$. It can be observed that, as the TMD is tuned to higher frequencies, the building-TMD system becomes stiffer, and oscillates as a rigid body, with the top floor displacement matching closely the imposed base displacements.

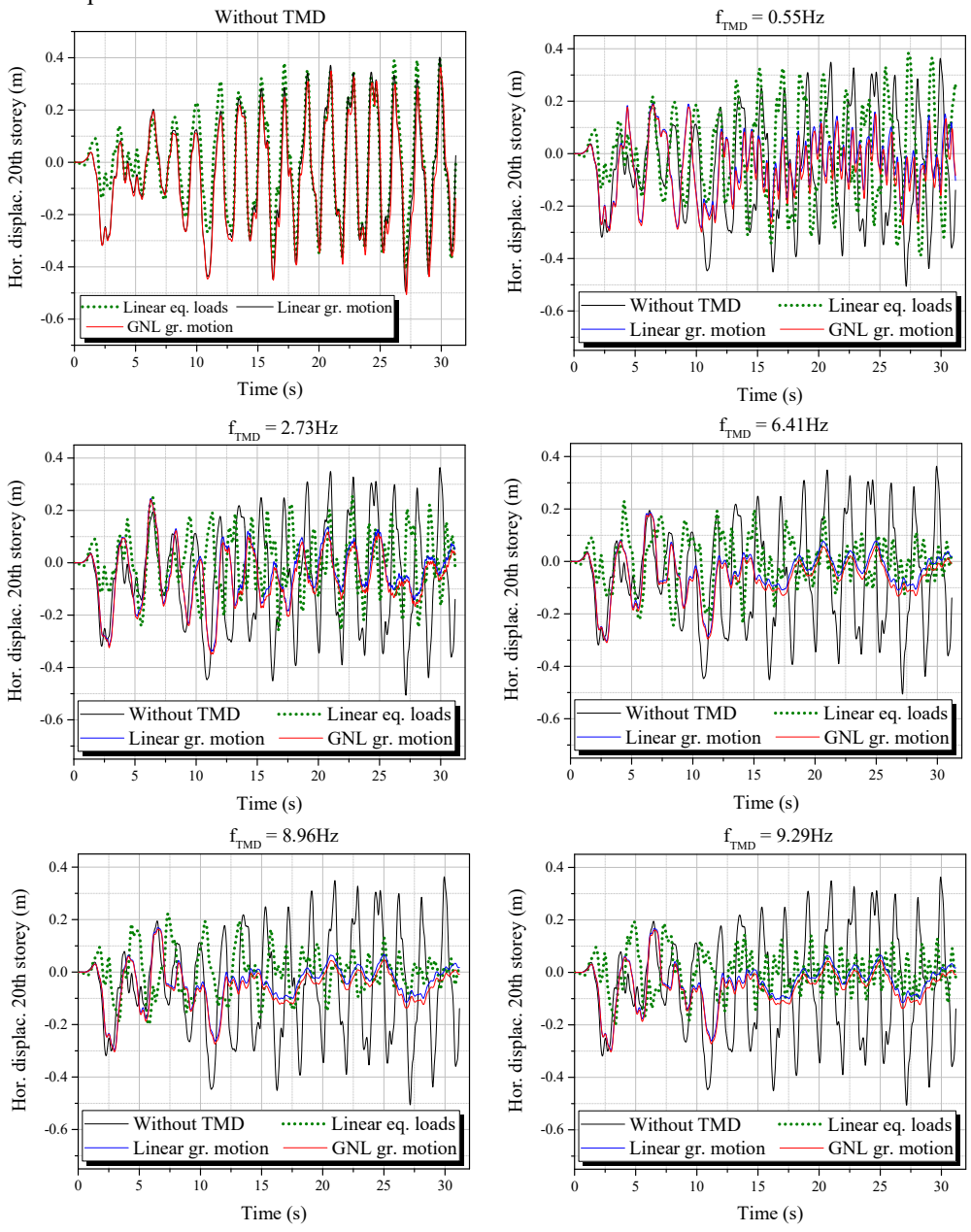

Figure 8 – Horizontal displacements at 20th storey, without and with TMDs tuned to different frequencies.

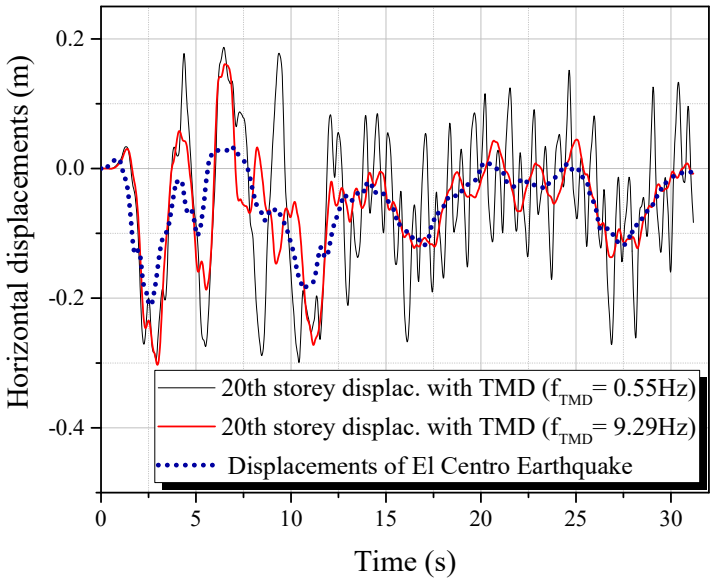

Figure 9 - Comparison between base-imposed and buildings last floor displacements, for two different TMDs.

CONCLUDING REMARKS

This paper pursued a dual objective: to investigate usual modelling assumptions and to study the performance of buildings equipped with Tuned Mass Damper (TMD) devices, when subject to earthquake loadings.

With respect to modelling assumptions, the simplified linear mass-spring model, frequently employed in the literature, was compared with linear and geometrical non-linear FE models. It was shown that the simple mass-spring models are very limited, and cannot accurately predict the natural frequencies nor the displacement responses of the structure. A linear FE model with equivalent nodal loads was also considered, and compared to a model of base-imposed displacements. It was found that the equivalent load model significantly underestimates building displacements, leading to oscillations around the initial position.

A linear FE model was also compared with a geometrical non-linear model, both considering base-imposed displacements. The non-linear model is a position-based FE model, where equilibrium is warranted at the final, displaced position. Both models presented similar results, showing that the structure subject of this study behaves in linear regime, with small to moderate displacements. Hence, for this particular structure, the more computationally intensive NL solution is not required. This study will be extended in the future to address buildings with large displacements.

Since earthquake loading excites different vibration modes of the structure, the tuning of TMD frequency is not obvious. In this paper, it was shown that for the El Centro earthquake loading, TMDs present better efficiency when tuned to higher natural frequencies of the structure. For the 20-storey building studied herein, the TMDs were capable of reducing displacement amplitudes and oscillatory frequency. This was observed mainly for TMDs tuned to the 8th natural frequency of the building (or higher). This is in contrast to what is commonly believed in the literature, i.e., that tuning the TMD to the first natural frequency is optimal. For the particular excitation of El Centro earthquake, results show that TMDs tuned to higher natural frequencies of the structure reduce displacements and oscillation frequencies guarantying more comfort to the building occupants when the building. For more general conclusions, this study will be extended to address structures under earthquakes simulated as stochastic processes in different types of soil.

The methodology proposed in this paper demonstrates the effectiveness of TMD devices in controlling structural vibrations of structures subject to earthquake loadings. However, benefits are only achieved when TMDs are properly tuned, and when structural responses are correctly evaluated. Simple lumped spring-mass models and linear equivalent load FE models are very limited in predicting structural responses under earthquake excitations, even for linear structures.

ACKNOWLEDGEMENTS

The authors acknowledge funding of this research project by Brazilian agencies CAPES (Higher Education Council) and CNPq (National Council for Research).

REFERENCES

Beck, A. T., et al., 2014. Optimal performance-based design of non-linear stochastic dynamical RC structures subject to stationary wind excitation, Engineering Structures, 78, 145–153.

Coda, H. B. and Greco, M., 2004. A simple FEM formulation for large deflection 2D frame analysis based on position description, Computer Methods in Applied Mechanics and Engineering, 193, 3541–3557.

Coda, H. B. and Paccola, R. R., 2014. A total-Lagrangian position-based FEM applied to physical and geometrical nonlinear dynamics of plane frames including semi-rigid connections and progressive collapse, Finite Elements in Analysis and Design, 91, 1–15.

Fhram, H., 1909. Device for damping vibration of bodies.

Hartog, D., 1928. The theory of dynamic vibration absorber. Transactions of the ASME.

Hoang, N., et al., 2008. Optimal tuned mass damper for seismic applications and practical design formulas, Engineering Structures, 30, 707–715.

Housner, G. W. et al., 1997. Structural Control : Past , Present , and Future, J. Eng. Mech, (September), 897–971.

Kaynia A. M. et al., 1981. Seismic Effectiveness of Tuned Mass Dampers. VERRR

Lazar, I. F. et al., 2014. Using an inerter-based device for structural vibration suppression, Earthquake Engineering & Structural Dynamics, 43(11), 1129–1147.

Miguel, L. F. F. et al. Robust design optimization of TMDs in vehicle-bridge coupled vibration problems, To appear in Engineering Structures, paper accepted August 2016.

Moutinho, C., 2012. An alternative methodology for designing tuned mass dampers to reduce seismic vibrations in buildings structures, Earthquake Engineering & Structural Dynamics, 41(11), 2059–2073.

Parulekar, Y. M. and Reddy, G. R., 2009. For Seismic Response Reduction, International Journal of Structural Stability and Dynamics, 9(1), 151–177.

Paultre, P., 2010. Dynamics of Structures. Igarss 2014 (1st ed.). Wiley & Sons, Inc.

Pourzeynali, S. et al., 2007. Active control of high rise building structures using fuzzy logic and genetic algorithms, 29, 346–357. VERRR

Rana, R. and Soong, T. T., 1998. Parametric study and simplified design of tuned mass dampers, Engineering Structures, 20(3), 193–204.

Silva, W. Q., 2010. Análise não linear geométrica do acoplamento solo-estrutura através da combinação MEC-MEF. University of São Paulo.

Soto-brito, R. and Ruiz, S. E., 1999. Influence of ground motion intensity on the effectiveness of tuned mass dampers, Earthquake Engineering & Structural Dynamics, 1271(May), 1255–1271.

Spencer, J. B. F. and Nagarajaiah, S., 2003. State of the Art of Structural Control, Journal of Structural Engineering, (July), 845–856.

Warburton, G. and Ayorinde, E., 1980. Optimum absorber parameters for simples systems, Earthquake Engineering & Structural Dynamics, 8, 197–217.

Warburton, G. B., 1976. The dynamical behaviour of structures (2nd ed.). Pergamom press.

Warburton, G. B., 1982. Optimum absorber parameters for various combinations of response and excitation parameters. Earthquake Engineering & Structural Dynamics, 10, 381–401.

RESPONSIBILITY NOTICE

The authors are the only responsible for the material included in this paper.